Dynamics of nonthermal states in optimally doped $Bi_2Sr_2Ca_{0.92}Y_{0.08}Cu_2O_{8+\delta}$ revealed by midinfrared three-pulse spectroscopy

Angela Montanaro,[1,2,3] Enrico Maria Rigoni,[1,2] Francesca Giusti,[1,2] Luisa Barba,[4] Giuseppe Chita,[4] Filippo Glerean,[5] Giacomo Jarc,[1,2] Shahla Y. Mathengattil,[1,2] Fabio Boschini,[6,7] Hiroshi Eisaki,[8] Martin Greven,[9] Andrea Damascelli,[7,10] Claudio Giannetti,[11,12,13] Dragan Mihailovic,[14] Viktor Kabanov,[14] and Daniele Fausti[1,2,3,*]

[1]*Department of Physics, Università degli Studi di Trieste, 34127 Trieste, Italy*
[2]*Elettra Sincrotrone Trieste S.C.p.A., 34149 Basovizza Trieste, Italy*
[3]*Department of Physics, University of Erlangen-Nürnberg, 91058 Erlangen, Germany*
[4]*Institute of Crystallography, CNR, Elettra Sincrotrone Trieste S.C.p.A., 34149 Basovizza Trieste, Italy*
[5]*Department of Physics, Harvard University, Cambridge, Massachusetts 02138, USA*
[6]*Centre Énergie Matériaux Télécommunications, Institut National de la Recherche Scientifique, Varennes, Québec, Canada J3X1S2*
[7]*Quantum Matter Institute, University of British Columbia, Vancouver, BC, Canada V6T 1Z4*
[8]*Research Institute for Advanced Electronics and Photonics, National Institute of Advanced Industrial Science and Technology, Tsukuba, Ibaraki 305–8568, Japan*
[9]*School of Physics and Astronomy, University of Minnesota, Minneapolis, Minnesota 55455, USA*
[10]*Department of Physics & Astronomy, University of British Columbia, Vancouver, BC, Canada V6T 1Z1*
[11]*Department of Mathematics and Physics, Università Cattolica, I-25121 Brescia, Italy*
[12]*Interdisciplinary Laboratories for Advanced Materials Physics (I-LAMP), Università Cattolica, I-25121 Brescia, Italy*
[13]*CNR-INO (National Institute of Optics), via Branze 45, 25123 Brescia, Italy*
[14]*Jožef Stefan Institute, Jamova 39, 1000 Ljubljana, Slovenia*

(Received 8 September 2023; revised 25 April 2024; accepted 29 July 2024; published 3 September 2024)

In the cuprates, the opening of a d-wave superconducting (SC) gap is accompanied by a redistribution of spectral weight at energies two orders of magnitude larger than this gap. This indicates the importance to the pairing mechanism of on-site electronic excitations, such as orbital transitions or charge transfer excitations. Here, we resort to a three-pulse pump-probe scheme to study the broadband nonequilibrium dielectric function in optimally doped $Bi_2Sr_2Ca_{0.92}Y_{0.08}Cu_2O_{8+\delta}$ and we identify an interband excitation peaked at 2 eV whose spectral weight is transiently modified by the pump. Photoexcitation with near-infrared and midinfrared pulses, with photon energies, respectively, above and below the SC gap, reveals that the spectral weight dynamics is different for different pump wavelengths and depends on the time order of the two photoexcitations. The picture that emerges is that, while high-energy pulses excite quasiparticles in both nodal and thermally inaccessible antinodal states, photoexcitation by low-energy pulses mostly accelerates the condensate and creates excitations predominantly at the nodes of the SC gap. These results, rationalized by simulations based on the kinetic equations for d-wave superconducting gaps, indicate that dynamical control of the momentum-dependent distribution of nonthermal quasiparticles may be achieved by the selective tuning of the photoexcitation.

DOI: 10.1103/PhysRevB.110.125102

I. INTRODUCTION

The interplay between the high- and low-energy electrodynamics is one of the unconventional features of cuprate superconductors. While in standard Bardeen-Cooper-Schrieffer (BCS) superconductors the opening of a superconducting (SC) gap (Δ_{SC}) triggers a rearrangement of the quasiparticle excitation spectrum only in an energy range that is comparable with $2\Delta_{SC}$ (a few tens of meV), the condensate formation in the cuprates is accompanied by a redistribution of spectral weight at energies that are two orders of magnitude larger than $2\Delta_{SC}$ [1–6]. This anomalous and still much-debated behavior hints at a direct involvement of the high-energy electronic excitations in the pairing mechanism of high-T_C superconductivity.

A further complication arises from the symmetry of the SC gap. Whereas standard BCS superconductors exhibit a fully symmetric s-wave gap that naturally emerges from phonon-mediated pairing, in the cuprates the gap has d-wave symmetry [7–10]. Whereas at the antinode electronic transitions are permitted only at frequencies larger than the SC gap, electronic excitations at all frequencies are allowed at the nodes, where the gap amplitude vanishes.

Understanding how the momentum distribution of the electronic excitations affects the d-wave SC gap is pivotal to advance the field and, arguably, a way to distinguish between the many microscopic models proposed for the cuprate superconductors [11–13]. This has stimulated a tremendous development of momentum-resolved experimental

*Contact author: daniele.fausti@fau.de

techniques, both equilibrium and their time-resolved counterparts [14–16].

When the cuprates are photoexcited by ultrashort laser pulses, excess quasiparticles (QPs) are injected into the system and perturb the initial equilibrium distribution [17–27]. While angle-resolved photoemission spectroscopy (ARPES) studies indicate that high-photon energy pulses (>1.5 eV) excite a QP population uniformly distributed across the Fermi surface [26,28], the effect of the photoexcitation by low-photon energy pulses (i.e., smaller than the SC gap) has been less investigated [29]. Evidence for transient SC phases triggered by long-wavelength electric fields has been reported [30–35], suggesting that excitation by pulses with photon energy smaller than the SC gap may lead to different transient electronic states.

To disentangle the effects of high- and low-photon energy excitations, here we employ a three-pulse scheme that combines a near-infrared pump (near-IR, $h\nu_{\mathrm{NIR}} \gg 2\Delta_{\mathrm{SC}}$), a midinfrared pump (mid-IR, $h\nu_{\mathrm{MIR}} \leqslant 2\Delta_{\mathrm{SC}}$), and a white-light probe ($1.5 < h\nu < 2$ eV). The rationale of our approach is to first use one pump to drive the system into a nonthermal state, and then to measure the subsequent QP dynamics with the second pump-probe sequence. The broadband detection window enables the measurement of the transient high-energy dielectric function of the sample, and thus allows us to directly probe the involvement of the high-energy electronic excitations in that spectral range.

We find that the transient response in optimally doped $Bi_2Sr_2Ca_{0.92}Y_{0.08}Cu_2O_{8+\delta}$ (Y-Bi2212) below T_C can be fully accounted for by a blueshift and an impulsive change of spectral weight of an interband excitation peaked at 2 eV. Importantly, while the blueshift dynamics is qualitatively the same regardless of the choice of the pump and the sample temperature, the dynamics of the spectral weight (*SW*) is sensitive to both the pump photon energy and the pump polarization and displays a clear signature of the onset of the SC state.

We use the *SW* dynamics as an observable to study the response of the sample to subsequent excitations by the near-IR and the mid-IR pumps. We observe that the double-pump response depends on the order in which the two pumps impinge on the sample. When the system is first photoexcited by subgap pulses, the *SW* dynamics triggered by the near-IR pump is not affected by the presence of the previous photoexcitation. Conversely, photoexcitation by above-gap pulses strongly modifies the dynamics later initiated by the mid-IR pump, which becomes similar to the one triggered by high-energy pulses. The measurements can be qualitatively rationalized within a theoretical framework based on the kinetic equations for superconductors [36–38], which can discriminate between the effects of low- and high-frequency photoexcitations on the momentum-resolved distribution function of nonequilibrium QPs.

The manuscript is organized as follows. The experimental technique combining mid-IR and near-IR pumps with a broadband probe is presented in Sec. II. Section III reports the main experimental evidence and the discussion of our results. The visible spectral response of Y-Bi2212 is discussed in Sec. III A, the dynamical response to single photoexcitation at different pump wavelength in the SC phase in Sec. III B, and in the normal and pseudogap phase in Sec. III C. The temperature dependence of the response to photoexcitation with single pump is discussed in Sec. III D, while the double-pump measurements and kinetic model are reported and discussed in Secs. III E and III F, respectively.

II. EXPERIMENTAL METHODS

We carried out time-domain optical measurements on a freshly cleaved sample of optimally doped Y-Bi2212 at different temperatures. The sample displays a SC phase below $T_C = 96$ K [39], and a pseudogap (PG) phase between T_C and $T^* \cong 135$ K; above T^*, the system behaves as a "strange metal". The absolute value of the d-wave gap in reciprocal space is sketched in Fig. 1(d). The antinodal gap amplitude is $2\Delta_{\mathrm{SC}} \sim 75$ meV [40].

The three-pulse optical setup is sketched in Fig. 1(a). The sample is simultaneously photoexcited by a near-IR pump ($1.44\ \mathrm{eV} \gg 2\Delta_{\mathrm{SC}}$) generated by a noncollinear parametric amplifier system and a mid-IR pump ($70\ \mathrm{meV} \leqslant 2\Delta_{\mathrm{SC}}$) obtained through difference frequency generation of two near-IR pulses coming from a twin optical parametric amplifier system. The transient broadband reflectivity is probed by a white-light supercontinuum (1.5–2 eV) obtained through self-phase modulation in a sapphire crystal. The three pulses propagate along the c axis (orthogonally to the Cu-O plane). The pump beams are copolarized, while the probe polarization is orthogonal to the pumps. This cross-polarized configuration was chosen to filter out the scattered near-IR pump light by means of an analyzer orthogonal to the pump polarization. The polarization of the impinging beams with respect to the CuO_2 plaquette can be adjusted by rotating the sample with a piezoelectric rotator in the vacuum chamber. The sample has been oriented through x-ray diffraction measurements at the beamline XRD1 at Elettra Sincrotrone Trieste. More details on the experimental setup can be found in Ref. [41].

The two optical choppers placed along the pumps' optical paths run such that one is twice as fast as the other. A proper sorting of the probe pulses according to the choppers' rotational frequencies allows to single out (i) the response to only the near-IR pump; (ii) the response to only the mid-IR pump; (iii) the joint response to both the photoexcitations. As illustrated in Fig. 1(b), for each given delay $\bar{t}$ of the probe beam, the broadband transient change in reflectivity induced by the pumps is measured. By tuning the time delay $\tilde{T}$ between the pump pulses, the order of arrival of the pumps can be swapped. This allows us to determine, within the same measurement, how the photoexcitation by the first impinging pump modifies the dynamics measured by the second pump-probe sequence.

III. RESULTS AND DISCUSSION

A. Equilibrium optical properties of Y-Bi2212

The equilibrium properties of the cuprates are mainly determined by the Cu $3d$ and the O $2p$ orbitals within the CuO_2 plaquette. In the insulating parent compounds, the strong on-site Coulomb repulsion splits the Cu $3d$ band into a lower and an upper (UHB) Hubbard band. The O $2p$ band, which is fully occupied, falls inside this gap, ∼2 eV below the UHB. The

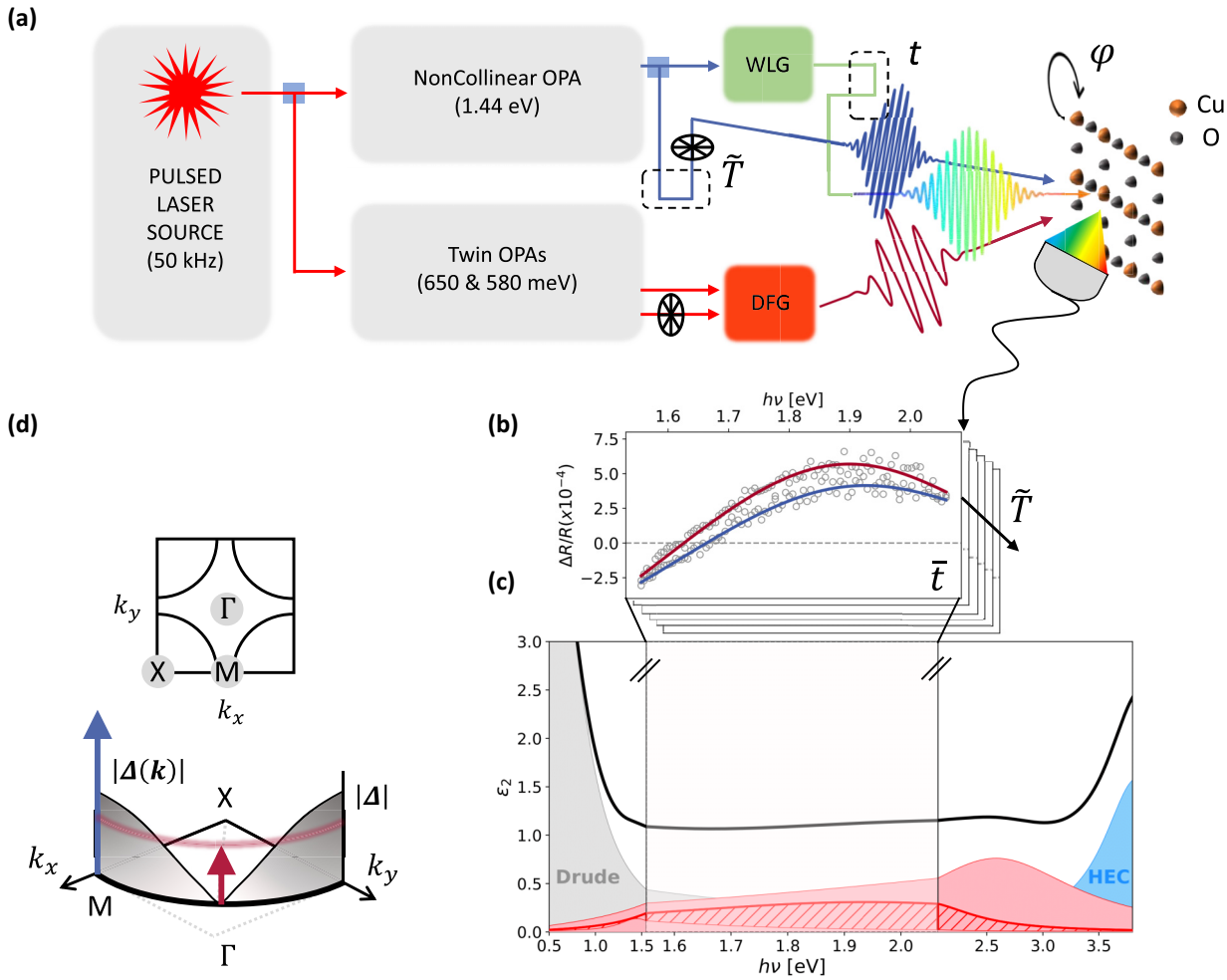

FIG. 1. Time-dependent broadband measurements of dielectric function upon photoexcitation above and below the superconducting gap. (a) Sketch of the three-pulse experimental setup. "WLG" stands for White-Light Generation, "DFG" for Difference-Frequency Generation. "$\tilde{T}$" indicates the delay between the two pumps, "t" the delay between the near-IR pump and the supercontinuum probe. The in-plane sample orientation (φ) can be adjusted by a piezoelectric rotator mounted. (b) Example of transient reflectivity spectra (grey circles) and corresponding differential fits to the data (solid lines) at fixed $\bar{t}$ for the near-IR (blue) and mid-IR (red) pumps, simultaneously acquired. This is representative of the full $\tilde{T}$ dynamics. (c) Imaginary part of the dielectric function obtained through a Kramers-Kronig constrained Drude-Lorentz fit [58] of the dielectric function of Y-Bi2212 at T = 20 K (data published in Ref. [46]). The grey-shaded area accounts for the Drude peak and includes the low-energy contributions. The blue-shaded area indicates the high-energy contributions (HEC). The red peaks correspond to the oscillators that overlap with our probe window. The red pattern indicates the oscillator at $\omega_0 = 2$ eV that is the focus of our studies. (d) First Brillouin zone and absolute value of the superconducting gap in the reciprocal space for a d-wave superconductor. The blue and the red arrows represent the photoexcitations above and below the gap, respectively.

transition from the O $2p$ band to the UHB, which is the lowest-energy one in the system, represents the charge-transfer (CT) of a Cu $3d_{x^2-y^2}$ hole to its neighbouring O $2p_{x,y}$ orbitals and marks the lower bound of the electron-hole continuum. Upon hole doping, the charge-transfer edge (Δ_{CT}) shifts at higher energies and the CT gap is filled with states [42,43]. The assignment of the excitations within the energy window spanning from 1.5 to 2 eV is still controversial. Based on dynamical mean-field calculations, it has been proposed that the interband excitations are mostly related to many-body hybridized Cu-O states, corresponding to the Zhang-Rice singlet states [44–46]. On the other hand, dd orbital transitions are also expected to give a contribution in the range 1.5–2 eV. Evidence for an excitation localized at these energies has been reported by Raman scattering experiments in a large number of undoped cuprate superconductors and attributed to the Raman-activated hole transition from the in-plane $d_{x^2-y^2}$ to the d_{xy} orbital with A_{2g} symmetry [47]. Furthermore, resonant inelastic x-ray scattering measurements showed that the dd orbital transitions dominate the excitation spectrum at these energies also in doped SC cuprates [48,49]. The recent observation of a modification of the dd spectrum upon entering the SC phase further emphasizes the role that these excitations may play in the pairing [50,51].

In Fig. 1(c), we plot the imaginary part of the dielectric function of an optimally doped Y-Bi2212 sample measured at T = 20 K by spectroscopic ellipsometry (adapted from Ref. [46]). While the low-energy side ($h\nu < 1.25$ eV) of the dielectric function is dominated by the tail of the Drude response of the itinerant carriers and by lower-energy mid-IR

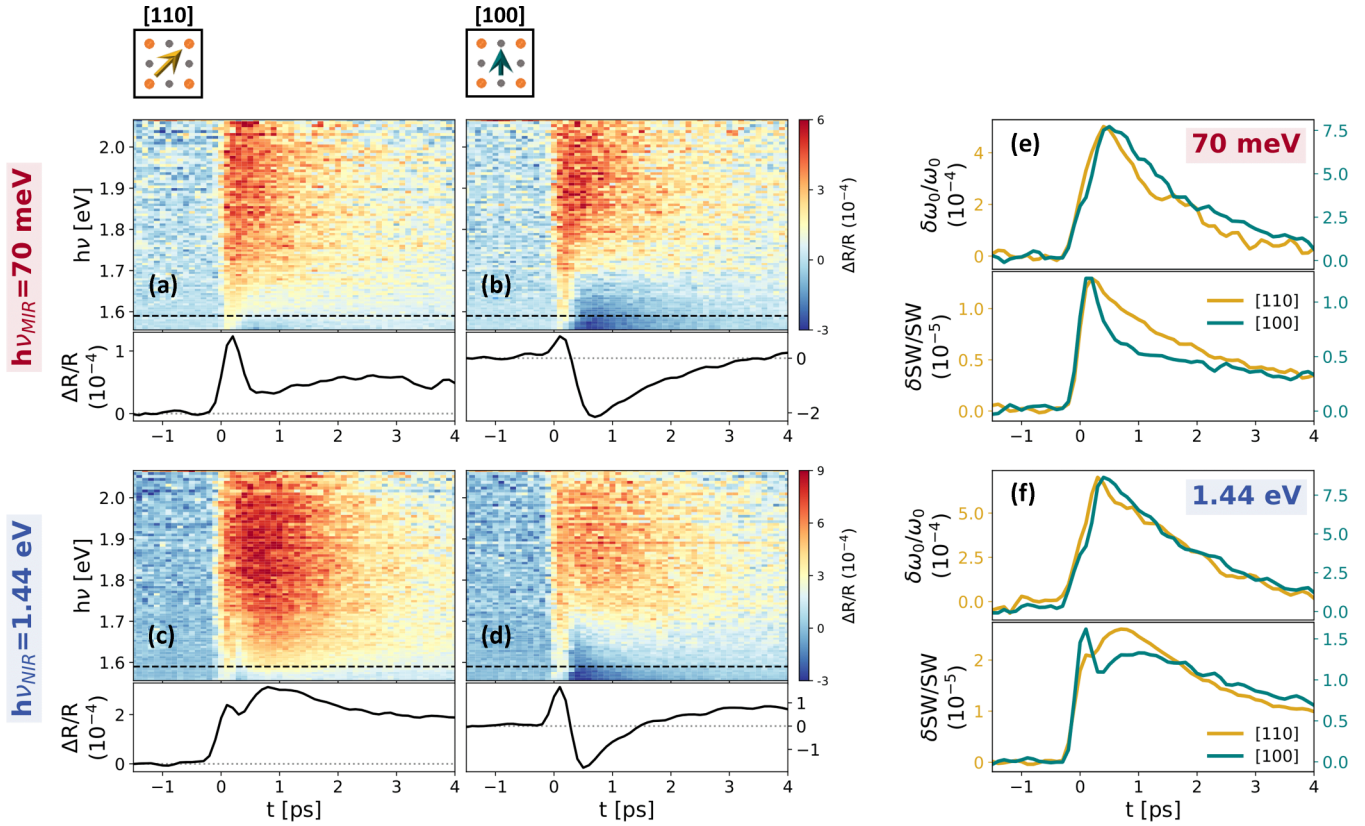

FIG. 2. Polarization-dependent pump-probe measurements for below- and above-gap photoexcitation in the superconducting phase. (a),(b) Broadband transient reflectivity upon a photoexcitation by mid-IR pulses (70 meV) with a pump pulse polarized along [110] and [100], respectively. The black line in the lower panels is a cut at 1.59 eV. The fluence of the mid-IR pump was $\varphi_{\mathrm{MIR}} = 28\,\mu\mathrm{J/cm}^2$ and the sample temperature was T = 74 K. (c),(d) Same as (a),(b), but for a high-energy near-IR photoexcitation (1.44 eV) and fluence $\varphi_{\mathrm{NIR}} = 19\,\mu\mathrm{J/cm}^2$. (e) Results of differential fits of the measurements in (a) and (b), as described in the text. For both polarizations of the pump ([110] in gold and [100] in teal), the curves in the top panel show the transient change in the central frequency of the oscillator at $\omega_0 = 2$ eV, which is primarily responsible for the nonequilibrium response in the probed spectral region, as shown in Fig. 1(c). In the bottom panel, the curves represent the transient change in the integrated spectral weight (SW $\propto \int_0^{5eV} d\omega\, \omega\, \varepsilon_2(\omega)$,) for the two pump polarizations. (f) Same as (e), but for the near-IR photoexcitation.

contributions, the high-energy side is reminiscent of a CT-like absorption edge ($h\nu > 2.5$ eV). The interband transitions give rise to a structured absorption in the region extending from 1.25 to 2 eV. As indicated by the grey-shaded area, our broadband probe overlaps with this window, directly enabling the measurement of the impulsive modification of these states.

In order to quantitatively estimate the pump-induced changes in the electronic excitations, we fitted the static dielectric function of the material using a Drude-Lorentz model (see Supplemental Note 1 in Supplemental Material [52]) consisting of a Drude peak (ε_D) and a sum of Lorentzian oscillators to account for the electronic transitions ($\sum_i \varepsilon_L^i$). In agreement with Ref. [46], we found that three oscillators are sufficient to fit the dielectric function in the energy range 1.25–2 eV and they correspond to the three red Lorentzian peaks in Fig. 1(c). We highlight with a red pattern the transition peaked at 2 eV that will be the focus of our time-domain studies. It is worth noting that the transitions extrapolated from the fit could also be made of several unresolved peaks, as the complexity of the optical spectra of the cuprates might suggest [45,59]. We thus stress that the Lorentzian peaks in Fig. 1(c) should be considered as an effective description rather than a physical microscopic modeling of the complex optical response of the sample. The discussion in the present work does not aim to clarify the nature of these excitations and will be limited to considering to what extent the high-energy physics is involved in the pairing.

B. Selective photoexcitation in the superconducting phase

The study of the dynamics in a tailored nonthermal state relies on the knowledge of the QP dynamics in the system that is initially at equilibrium. In this section, we focus on the characterization of the sample response to a single excitation with photon energy either below or above the SC gap.

In Figs. 2(a) and 2(c), we compare the broadband transient reflectivity upon photoexcitation in the SC phase by the mid-IR pump and the near-IR pump, respectively. The polarization of both pumps was parallel to [110], as illustrated in the top inset. The measurements were performed at low pumping fluences ($\phi < 30\,\mu\mathrm{J/cm}^2$) to avoid the complete vaporization of the condensate [19]. To guarantee a meaningful comparison between the signal at high- and low-pump photon

energy, we tuned the intensity of the pumps to have similar $\Delta R/R$ amplitude at fixed probe energy. Although the transient change in reflectivity is positive over the entire probe window (in agreement with the one measured in Ref. [46] with a 1.55-eV pump pulse), the dynamics of the signal displays a dependence on the photon energy of the pump. This difference is more pronounced at low probe energies, where the black cuts ($h\nu_{pr} = 1.59$ eV) in the lower panels of Figs. 2(a) and 2(c) are selected.

Motivated by the distinctive gap anisotropy of the sample and its anisotropic response to long-wavelength pulse excitation that we have recently reported [35,60], we investigated how the broadband response changes according to the polarization of the pump beams. In Figs. 2(b) and 2(d) we show the time- and spectrally resolved transient reflectivity for the pump polarizations parallel to the direction of the Cu-O bond ([100]). We observe that, in both maps, the transient reflectivity changes sign at approximately 1.7 eV and displays a negative dynamics below this threshold [black cuts in the lower panels of Figs. 2(b) and 2(d)]. We stress that reducing the pump and the probe fluences does not qualitatively affect the spectral dependence of the response in this polarization configuration (Fig. S1–S3 in Ref. [52]), confirming that the measurements are performed in the linear regime.

To understand the origin of the observed structured reflectivity, we performed a differential fit of the maps based on the equilibrium dielectric function ($\varepsilon_{eq}(\omega)$) discussed in Sec. III A. The key idea of the analysis is to modify the minimum number of parameters that model $\varepsilon_{eq}(\omega)$ in order to fit, at every time delay, the measured transient broadband reflectivity (see Supplemental Note 2 for details on the fitting procedure [52]). The analysis revealed that a transient change of only the Lorentzian oscillator peaked at 2 eV is sufficient to reproduce our data. In particular, we found that the photoexcitation results in a blueshift of the central frequency (ω_0) of this oscillator and in a change of the integrated spectral weight (*SW*), formally defined as $SW \propto \int_0^{5eV} d\omega\, \omega\, \varepsilon_2(\omega)$, where we performed the integration over the whole energy axis of the fitted $\varepsilon_{eq}(\omega)$ (Supplemental Note 1 in Ref. [52]). We stress that the dynamics of ω_0 and *SW* are uncorrelated and thus these two parameters constitute a good pair of candidates to consistently describe the measurements (Supplemental Note 2 in [52]).

We show in Figs. 2(e) and 2(f) the results of the differential fits for photoexcitation with pulse photon energy below and above $2\Delta_{SC}$, respectively. We plot the relative change $\delta\omega_0/\omega_0$ and $\delta SW/SW$ as a function of the pump-probe delay for both pump polarizations in each panel. Neither the pump photon energy nor the pump polarization have any influence on the dynamics of the blueshift: the dynamics in all the four combinations [curves in the top panels of Figs. 2(e) and 2(f)) can be well described by a single-exponential with a decay time equal to ∼1.5 ps.

The dynamics of the integrated *SW* is instead more peculiar. By comparing the curves in the bottom panels of Figs. 2(e) and 2(f), we observe a different dynamics depending on the pump used: when the sample is photoexcited by the above-gap pump [bottom panel in Fig. 2(f)], the *SW* dynamics displays a fast-decaying component and an additional peak emerging at later times; the latter peak is instead absent in the *SW* dynamics initiated by the subgap pump [bottom panel in Fig. 2(e)].

It is interesting to note that the behavior in the bottom panel of Fig. 2(f) is reminiscent of the dynamics of the transient single-color reflectivity (at 1.55 eV) measured in other works upon photoexcitation by above-gap pumps [19,61]. In particular, the fast peak is commonly ascribed to the incipient melting of the SC phase due to the sudden photoinjection of hot QPs that nonthermally lead to the filling of the gap [62,63]. The emergence of the second peak, which is farther delayed in time the more intense the photoexcitation is, is instead usually associated with the recovery dynamics of the condensate. In Bi2212, this has been observed to set in within a few ps [64]. However, this peculiar transient reflectivity response is not a generic sample's response and ultimately depends on the experimental parameters, such as probe photon energy and polarization [61,65]. Here, by fitting the transient dielectric function and thereby overcoming the limitations intrinsic to single-color pump-probe measurements, we show that this dynamics is directly mapped onto the variation of the integrated spectral weight (probe-energy independent quantity), and we thus confirm its general validity.

Interestingly, the absence of a second peak arising at later pump-probe delays in the mid-IR-induced *SW* change [bottom panel of Fig. 2(e)] may be an indication that the recombination is different in this case. It is generally accepted that excitation by high photon energy pulses uniformly targets the Fermi surface, leading to an accumulation of photoinjected QPs both at the nodes and at the antinodes of the SC gap [26,28]. However, as the double-pump measurements will show, photoexcitation by subgap pulses might not inject enough energy to excite QPs at the antinodes, leading to an anisotropic QP population mostly localized in the nodal regions of the Brillouin zone. We note that increasing the fluence of the mid-IR pump does not alter the dynamics of the photoinduced change in *SW* (Fig. S4 in Ref. [52]), which still lacks the recovery component at later times.

Finally, the *SW* dynamics is also affected by the pump polarization. For both pump photon energies, the dynamics is faster when the pump is polarized along [100], which corresponds to the antinodal direction. This further suggests that, in this condition, the photoinduced quench of the SC gap is more efficient [35,60].

C. Normal and pseudogap phase

The peculiar dependence of the broadband reflectivity on the photon energy and polarization of the pump pulse is a property of the SC phase. In Figs. 3(a) and 3(d) we show the time- and spectrally resolved reflectivity measured in the normal (T = 300 K) and the PG (T = 105 K) phase upon photoexcitation by the mid-IR pump polarized along [110]. The normal phase is characterized by a positive response that decays faster than the one in the SC phase. This is consistent with the literature [66] and generally attributed to the suppression of recombination processes due to the opening of the gap below T_C. In Figs. 3(b) and 3(c) we plot the time trace at $h\nu_{pr} = 1.63$ eV measured for both the pump polarizations and photon energies. The temporal traces at the same probe energy at T = 105 K [Figs. 3(e) and 3(f)] indicate that the transient reflectivity in the PG phase is qualitatively the same in all the

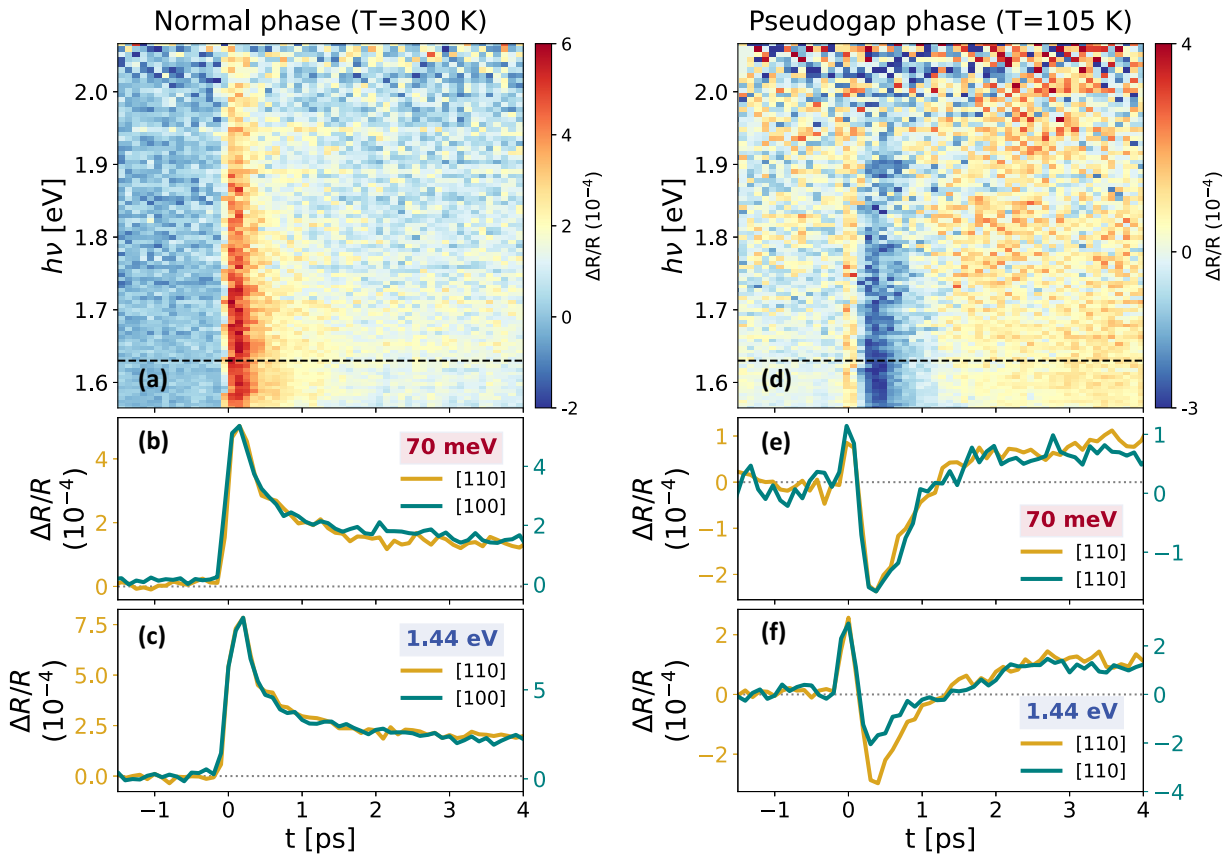

FIG. 3. Subgap pump-probe measurements in normal and pseudogap phases. (a) Transient reflectivity map at T = 300 K upon photoexcitation by the mid-IR pump polarized along [110] ($\varphi_{\mathrm{MIR}} = 28\,\mu\mathrm{J/cm}^2$). (b), (c) Horizontal cuts at 1.63 eV for the mid-IR and the near-IR pump, respectively. In each panel, the golden curve refers to the pump polarized along [110] and the teal curve for the pump polarized along [100]. (d)–(f) Same as (a)–(c), but in the pseudogap phase at T = 105 K.

configurations. After an initial positive peak, the reflectivity is negative; after ∼2 ps, a positive signal is restored. The lack of any pump dependence of the signal further suggests that the anisotropies emerging in the SC phase (Fig. 2) are associated with the symmetry of the SC gap.

Similar to the differential analysis carried out in the SC phase, we fitted the maps in Figs. 3(a) and 3(d) based on the dielectric function measured at T = 300 K and T = 100 K in Ref. [46]. Our analysis shows that, if the interband oscillators are arbitrarily frozen, the transient reflectivity above T_C can be fitted by modifying only the effective scattering rate of the Drude peak (Γ_D) in the dielectric function (Supplemental Note 3 in Ref. [52]), in agreement with other works [25,46,67].

This outcome, however, poses the delicate question of how to deal with the superconducting-to-pseudogap transition. When the PG phase is approached from higher temperatures, one effective parameter (Γ_D) would seem sufficient to track the transition from the normal phase. This is not the case at T_C, where the differential fits instead suggest a discontinuity in our model. By performing temperature-dependent measurements across the SC transition, we will show in the next section that a transient change of both the central frequency and the spectral weight of the 2 eV oscillator can equivalently account for the signal in the PG phase. However, the bandwidth of our measurements is not sufficient to conclusively address this question.

D. Nonequilibrium response across the superconducting phase transition

In Fig. 4(a), we plot the relative reflectivity variation as a function of the pump-probe delay (horizontal axis) and the sample temperature (vertical axis) across the SC transition. As an example, we plot here only the response to the subgap pump polarized along [110] and refer to Figs. S5,S6 in Ref. [52] for a complete characterization of the temperature-dependent response under other experimental conditions. At each temperature, the broadband response of the sample is measured by the white-light probe [Fig. 4(b)] and we select one specific probe energy (1.7 eV) to plot the color-coded map in Fig. 4(a). A clear discontinuity near T_C is present, where the signal changes sign. However, this is not a universal feature of the optical response: by changing either the pump or the probe photon energy and the pump polarization, the signal qualitatively changes (Figs. S5,S6 in Ref. [52]) and the SC transition cannot be readily inferred from the optical measurements.

We fitted the reflectivity maps using the model described in Sec. III A (Fig. S7 in Ref. [52]). The results of the

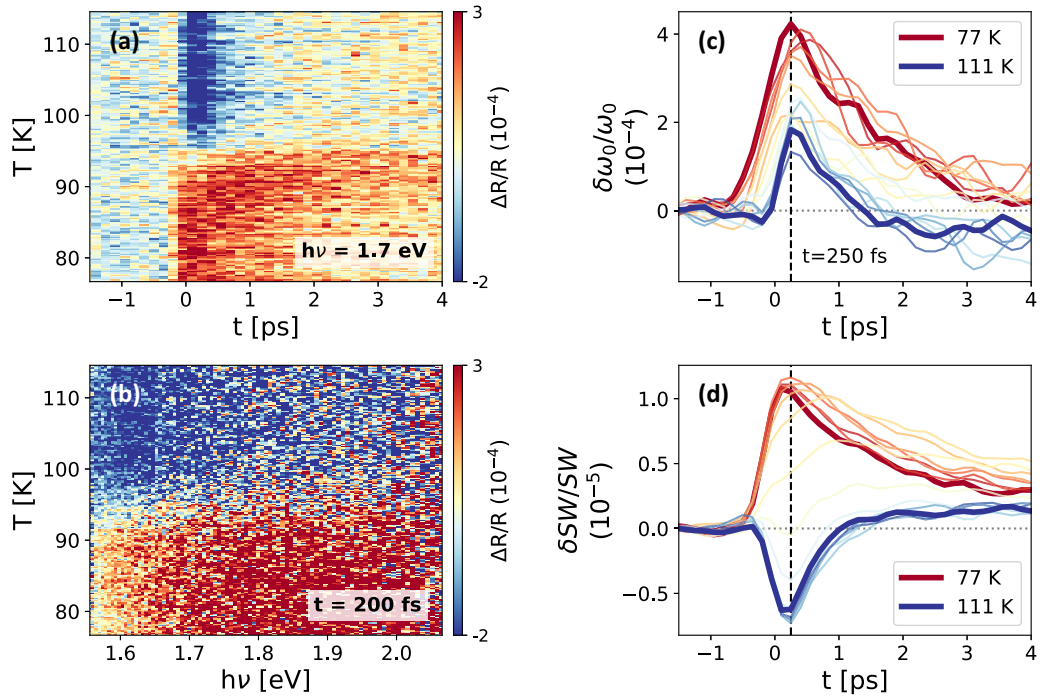

FIG. 4. Temperature-dependent dynamics of the interband excitation. (a) Transient reflectivity as a function of temperature and time delay at fixed probe energy (1.7 eV) upon photoexcitation by the mid-IR pump polarized along [110] ($\varphi_{\mathrm{MIR}} = 28\,\mu\mathrm{J/cm}^2$). (b) Same as (a) but as function of temperature and probe energy at fixed time delay (200 fs). (c) Time-dependent transient change in the central frequency of the $\omega_0 = 2$ eV oscillator for selected temperatures measured in (a). (d) Time-dependent transient change in spectral weight for selected temperatures in (a).

analysis are plotted in Figs. 4(c) and 4(d), where we show the dynamics of ω_0 and SW, respectively, of the 2-eV transition at different temperatures, from the SC phase (red curves) to the PG one (blue curves). The dynamics of the central frequency of the oscillator does not display a strong dependence on the temperature and remains positive also above T_C. This is in contrast to the SW dynamics, which changes sign when T_C is approached.

In Fig. 5, we plot the central frequency and the integrated spectral weight as a function of temperature associated with the maximum pump-induced change (t = 250 fs). From the main panels of Figs. 5(a) and 5(b), it is evident that the impulsive change of SW of the 2 eV interband oscillator is a good indicator of the SC transition. In contrast, the insets of Fig. 5 show the temperature dependence of the effective parameter ω_0, which reveals no transitions at T_C regardless of the pump photon energy and polarization.

This analysis emphasizes once again how the condensate formation is linked to the local high-energy excitations in the material [1,2,68,69]. In fact, it is known that in equilibrium a transfer of spectral weight from the high-energy spectral region to the zero-frequency δ function of the condensate occurs at T_C [4,70]. Following the same interpretation, the pump-induced spectral weight change we observe below T_C should be interpreted as a direct consequence of the quench of the SC pair density, which in our measurements does not appear to be directly related to the shift of the central frequency of the 2 eV oscillator.

In this respect, it is important to note that the dynamics of the central frequency of the oscillator at 2 eV and the integrated spectral weight in the visible range are indicative of two distinct processes, the first one independent of the presence of the condensate and the second one appearing only once three-dimensional superconductivity is observed. We conjecture that the light-driven shift of the oscillator is visible when the spectrum of electronic excitations is locally gapped, while the light-driven spectral weight dynamics is associated with the inductive response of the system which is related instead to the number of electrons in the condensate.

Interestingly, the excitation by above- and below-gap pumps yields different results. While high-photon energy pulses (regardless of their polarization) quench the condensate at temperatures lower than the equilibrium T_C [Fig. 5(b)], subgap pulses have an anisotropic effect [Fig. 5(a)]. When the mid-IR pump is polarized along [100], the quench is similar to the one induced by high-photon energy pulses. However, when the mid-IR polarization is parallel to [110], the discontinuity in the optical response associated to the SC transition occurs at 2–3 K higher temperatures [gold markers in Fig. 5(a)].

The scenario that emerges is consistent with the previous observation [35] of a superconductinglike response in single-color reflectivity measurements enhanced by mid-IR pulses polarized along [110]. In this regard, the employment of a broadband probe and thus the use of the integrated spectral weight as an observable (rather than the reflectivity at only one probe wavelength) enables us to provide a more general result. Importantly, our measurements highlight that the anisotropy of the subgap pulses arises from the anisotropic response of the high-energy electronic excitation to the perturbation, which in turn affects the dynamics of the condensate.

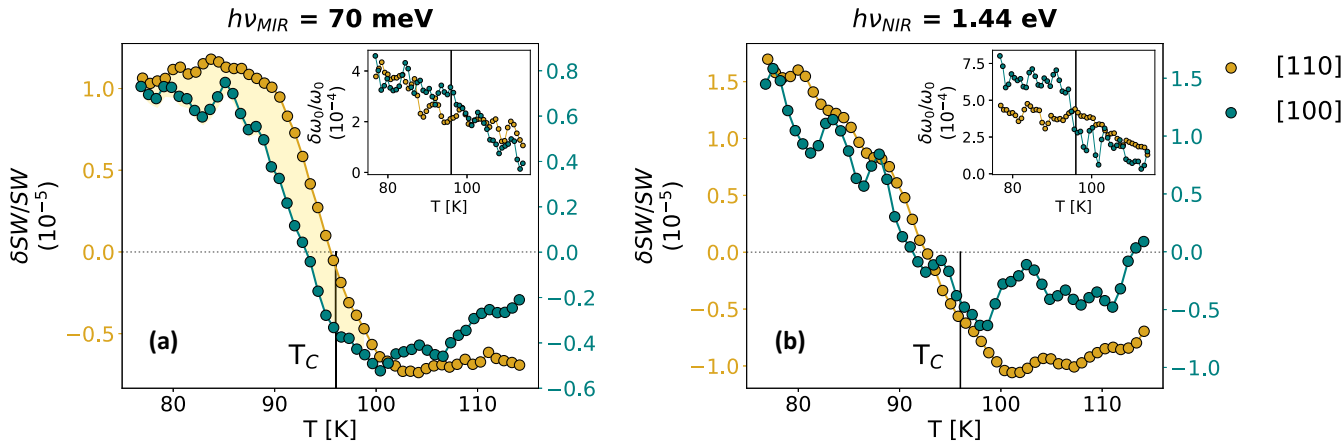

FIG. 5. Pump-induced change of the interband excitation across the superconducting transition. (a),(b) Transient change of the spectral weight of the 2 eV oscillator at t = 250 fs as function of temperature induced by the below- and the above-gap excitation, respectively, polarized along [110] (gold) and [100] (teal). The black vertical lines indicate the critical temperature. The insets show the temperature-dependent transient change of the central frequency of the oscillator at t = 250 fs.

E. Optical response of nonthermal states

In order to understand the origin of the different spectral weight dynamics to the near-IR and the mid-IR pumps, we employ here a three-pulse technique which consists in the subsequent excitation of the sample by two pump pulses. The rationale of this approach is that, depending on the photon energy of the first pump, the resulting nonthermal QP distribution across the Brillouin zone is expected to be different. A second pump-probe sequence is then employed to measure the broadband transient response of the photoinduced nonthermal state. We delay the second pump-probe sequence by 1 ps with respect to the first pump: this choice guarantees that the initially excited QPs are not completely relaxed before the arrival of the second pump [64] and, at the same time, avoids possible coherent artefacts arising from a temporal overlap of the two pumps. We plot in Fig. 6 the results of these measurements. For clarity, we show only the dynamics of the *SW* obtained through the differential fits, as we observed no difference in the dynamics of the ω_0 of the 2 eV oscillator (Fig. S11 in Ref. [52]). Moreover, we restrict here our discussion to the effect of the pumps polarized along [100], but the experimental findings are the same for the other pump polarization (Fig. S10 [52]). We refer to Fig. S9 in Ref. [52] for a complete set of the measured reflectivity maps.

The first row in Fig. 6 reports − as a reference − the single-pump *SW* dynamics initiated by the (a) above- and (b) subgap excitation in the SC phase [reproduced from Figs. 2(e) and 2(f)]. In the second row, we plot the *SW* dynamics obtained in the double-pump experiment: in (c) we report the near-IR induced *SW* dynamics measured in the sample previously excited at t =–1 ps by the subgap pulse; in (d) the order of the pumps is swapped, and we plot the mid-IR *SW* dynamics measured after the above-gap excitation.

The comparison of the *SW* dynamics photoinduced by the high-photon energy pulses with or without the previous interaction with the low-photon energy pump reveals that the dynamics is not significantly affected by the initial state of the sample, be it initially in equilibrium or previously driven into a nonthermal state by the excitation with the subgap pump [Fig. 6(c)]. On the contrary, if the order of the two pumps is reversed (i.e., the near-IR pump prepares a nonthermal state that is then probed by the mid-IR pump-probe sequence) the *SW* dynamics is markedly different [Fig. 6(d)]. When a QP population is excited by the above-gap pump, the *SW* dynamics revealed by the subgap pump is qualitatively similar to the one measured by the near-IR pump only, featuring an initial fast-decaying response superimposed to a slower delayed recovery dynamics.

Importantly, this difference is a peculiar property of the SC phase. In Figs. 6(e) and 6(f), we plot the differential reflectivity ($\Delta\Delta R/R$) across the SC phase transition, obtained as the difference between the double-pump response in Figs. 6(c) and 6(d) and the single-pump response in Figs. 6(a) and 6(b) for the near-IR and the mid-IR photoexcitation, respectively. In both cases, the differential signal vanishes above T_C (dashed black line), indicating that the response to double-excitation is equivalent to the sum of the two single-pump experiments above the critical temperature.

F. Kinetic-equation description of the electron dynamics

1. Theory

In order to rationalize these results in a comprehensive framework, we resorted to the quasiclassical kinetic theory initially derived for conventional superconductors [36,37,71,72] and later extended to anisotropic gaps by Kabanov and coworkers [38]. The leading idea of the model is to describe the effect of the photoexcitation as a sudden injection of excess QPs that perturb the equilibrium distribution function. The subsequent QP recombination dynamics is governed by the emission and reabsorption of high-frequency phonons, while low-frequency phonons do not take part directly in the relaxation process. Importantly, the model relies on the assumption that the density of photoexcited QP is

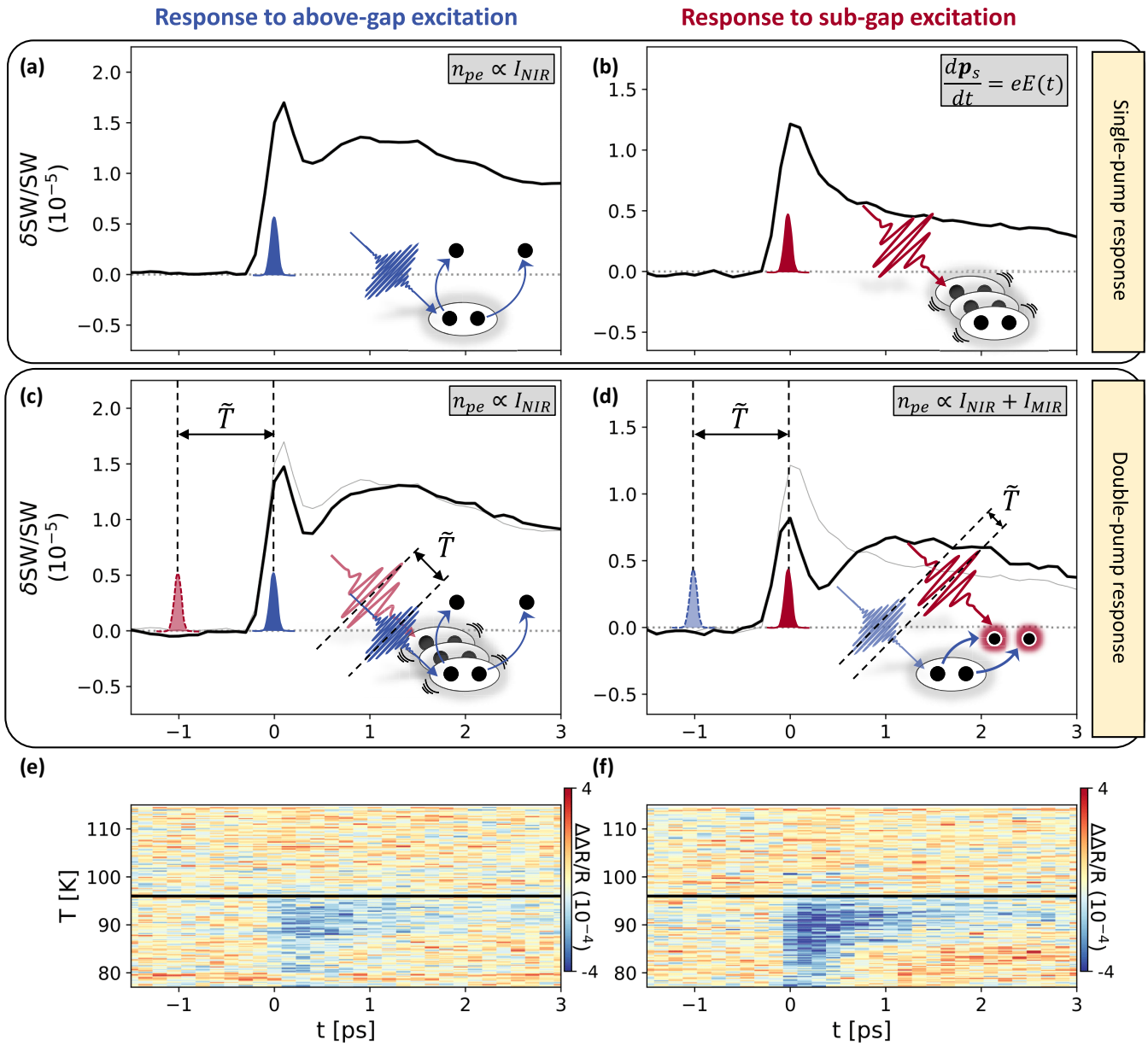

FIG. 6. Nonthermal quasiparticles in superconducting phase upon photoexcitation by above- and subgap pulses. (a), (b) Spectral weight dynamics extrapolated from the single-pump response to the above- and the subgap pulse, respectively [same as Figs. 2(e) and 2(f)]. The polarization of the pumps is parallel to [100] and the sample temperature is 74 K. (c) Spectral weight dynamics (black line) measured by the above-gap pulse when the system has been previously photoexcited by the mid-IR pulse at t =−1 ps (red Gaussian curve). The response to the first impinging pump at t =−1 ps was subtracted from the data. (d) Spectral weight dynamics (black line) measured by the subgap pulse in a sample that has previously (at t =−1 ps) interacted with the near-IR pulse. Grey curves in (c) and d) are the single-pump spectral weight dynamics displayed in (a) and (b). The drawings (bottom right in the panels) explain how the quasiparticle distribution is affected by the single or the double excitation. The equations (top right panels) summarize the main results of the kinetic model. (e), (f) Temperature-dependent differential signal obtained by subtracting the single-pump responses [in (a) and (b), respectively] from the double-pump response measured with both pumps [in (c) and (d), respectively]. The time in the map (horizontal axis) is the delay between the second pump and the white-light probe, while $\tilde{T}$ (delay between the two pumps) is fixed to 1 ps.

significantly smaller than the normal state carrier density, i.e., the photoexcitation is weak and does not fill the SC gap with states. In this respect, the pump fluence studies revealing a linear dependence of the transient signal on the pump intensity (Fig. S1, S2 in Refs. [52]) ensure the validity of this assumption in our measurements. Formally, the kinetic equations describing the QP (f_ϵ) and the phonon (N_q) distribution functions can be written in the form:

$$\frac{\partial f_\epsilon}{\partial t} + \frac{\partial \epsilon_p}{\partial p}\frac{\partial f_\epsilon}{\partial r} - \frac{\partial \epsilon_p}{\partial r}\frac{\partial f_\epsilon}{\partial p} = I\{f_\epsilon\} + Q$$
$$\frac{\partial N_q}{\partial t} = I_{ph-ph}\{f_\epsilon\} + I_{ph-e}\{f_\epsilon\}. \quad (1)$$

In the first equation, $\epsilon_p = \sqrt{\varepsilon_p^2 + \Delta_{\rm SC}^2} + \boldsymbol{p}_s \boldsymbol{v}$ is the energy of the QP, where, in addition to the usual energy dispersion involving $\varepsilon_p = \frac{p^2}{2m} - \mu + \phi + \frac{p_s^2}{2m}$ and the SC gap $\Delta_{\rm SC}$, we included the kinetic energy related to the movement of the condensate in its coordinate system [71]. In the notation used, μ is the chemical potential, ϕ is the electrostatic potential and $\boldsymbol{p}_s$ is the condensate momentum. We have denoted by Q the source of QP in the system (i.e., the photoexcitation) and with $I\{f_\epsilon\} = I_{im} + I_{e-ph} + I_{ee}$ the collision integrals describing, respectively, collisions between QP and impurities, QP and phonons and electroelectron collisions. In the second equation, the first term on the right-hand side is the phonon-phonon collision integral for anharmonic processes and the second term the collision integral describing the collisions of phonons with Bogoliubov QP.

We will now see how, depending on the photon energy $h\nu$ of the excitation with respect to the amplitude of the antinodal SC gap, we can discriminate two cases, eventually leading to two different physical scenarios: $h\nu \gg 2\Delta_{\rm SC}$, that is the case of the near-IR excitation in our experiment; $h\nu < 2\Delta_{\rm SC}$, that corresponds to the mid-IR excitation.

The effect of high-energy fields ($h\nu \gg 2\Delta_{\rm SC}$) has been widely studied in literature. Since the photon energy is larger than the antinodal gap, the high-energy pump is very efficient in creating QPs and subsequently breaking Cooper pairs; therefore, the leading term in Eq. (1) is Q. We sketched the expected pump-induced Cooper pair breaking in the bottom right of Fig. 6(a). If the temporal duration of the pump is shorter than the relaxation processes, Q determines the initial distribution of QPs. Furthermore, in the limit in which the electron-electron collisions and the electron-phonon recombination processes quickly lead to the phonon bottleneck [73], the distribution functions for phonons (N_{ν_q}) and quasiparticles (f_ϵ) can be, respectively, approximated as [38,74]:

$$N_{\nu_q} = \begin{cases} \frac{1}{e^{\frac{h\nu_q}{k_B T}} - 1}, & h\nu_q < 2\Delta_{\rm SC} \\ \frac{1}{e^{\frac{h\nu_q}{k_B T^*}} - 1}, & h\nu_q > 2\Delta_{\rm SC}, \end{cases} \tag{2}$$

$$f_\epsilon = \frac{1}{e^{\frac{\epsilon}{k_B T^*}} + 1}, \tag{3}$$

where T is the temperature of the low-frequency phonons ($h\nu_q < 2\Delta_{\rm SC}$, i.e., the lattice temperature) and T^* is the temperature of QP and high-frequency phonons ($h\nu_q > 2\Delta_{\rm SC}$). This approximation, that is equivalent to the model introduced in Ref. [75], entails that the relaxation of the bottleneck is ruled by the escape of high-frequency phonons below the gap via phonon-phonon collisions, as in the Rothwarf-Taylor description [76]. By imposing the conservation of energy, the photoexcited QP density (n_{pe}) can be derived and, in the case of a temperature-dependent gap $\Delta(T)$ that best describes the recombination rates in optimally doped cuprate samples [38], it is given by

$$n_{pe} = \frac{\mathcal{E}_I / \left(\Delta(T) + k_B T/2\right)}{1 + \frac{2\nu}{N(0)\Omega_c}\sqrt{\frac{2k_B T}{\pi \Delta(T)}} e^{-\frac{\Delta(T)}{k_B T}}}, \tag{4}$$

where $\mathcal{E}_I$ denotes the absorbed energy density of the high-energy pump pulse, ν is the effective number of phonon modes per unit cell involved in the recombination processes, $N(0)$ is the density of states at the Fermi energy and Ω_c is the phonon frequency cutoff. The temperature dependence of the photoexcited QP density in Eq. (4) highlights two important aspects: (i) the QP density n_{pe} scales linearly with the intensity of the high-energy pump; (ii) n_{pe} is expected to approach zero when the temperature reaches T_C. The good agreement found in optimally doped YBCO samples between theory and single-color 1.5-eV pump-probe transmission measurements confirms the efficacy of the model [38]. We included the expected linear dependence of the photoexcited QP density from the intensity of the near-infrared pump ($I_{\rm NIR}$) in our experiment in the top right of Fig. 6(a).

The case of low-energy fields ($h\nu < 2\Delta_{\rm SC}$) is instead very different. Looking back at the first row in Eq. (1) and considering a spatially uniform photoexcitation (so that all gradients vanish, except for the gradient of the electrostatic potential), the effect of low-energy excitations enters the kinetic equation via the gradient in the third term on the left-hand side of Eq. (1). As subgap pulses do not deliver sufficient energy to break Cooper pairs, the number of QPs is conserved following the photoexcitation. As a consequence, the main effect of this pump is limited to the acceleration of the condensate, as depicted in the bottom right of Fig. 6(b) and formally described by the equation [71,74,77]:

$$\frac{d\boldsymbol{p}_s}{dt} = eE(t), \tag{5}$$

where $E = -\nabla\phi$ is the electric field. In conventional s-wave superconductors, Eq. (5) leads to oscillation of the supercurrent, but it does not produce new QPs; at finite temperature, irradiation by subgap pulses can promote the already present thermally excited QPs to higher-energy empty states. This redistribution of the Bogoliubov excitations into a more favorable nonequilibrium distribution can eventually lead to an enhancement of superconductivity, known as the "Eliashberg effect" [78], that has been experimentally observed in superconducting thin films irradiated by THz pulses [79].

It should be highlighted, however, that this description might differ in the case of d-wave superconductors: pumps with photon energy smaller than the antinodal gap can still create QPs in the nodal directions. However, this effect is rather small, as the QP density of states within the gap is substantially suppressed, leading to a smaller probability of Cooper pair-breaking processes.

2. Simulations

The effect of the photoexcitation with subgap pulses does therefore depend on the initial state of the sample. If the sample is in equilibrium before the excitation, the dynamics is ruled by the thermal distribution of QPs. In Fig. 7(a), we simulate the momentum- and temperature-resolved QP population in equilibrium, obtained by multiplying the d-wave QP density of states [80] by the Fermi-Dirac distribution. In the calculations, we have parametrized the gap energy dispersion in momentum space as $\Delta(k) = \Delta_{\rm SC}\sin(ka)$, where $\Delta_{\rm SC}$ is the amplitude of the antinodal gap. In this parametrization, $ka = 0$ indicates the nodal direction and $ka = \pi/2$ the antinodal direction. As expected, at low temperatures $T/T_C \ll$

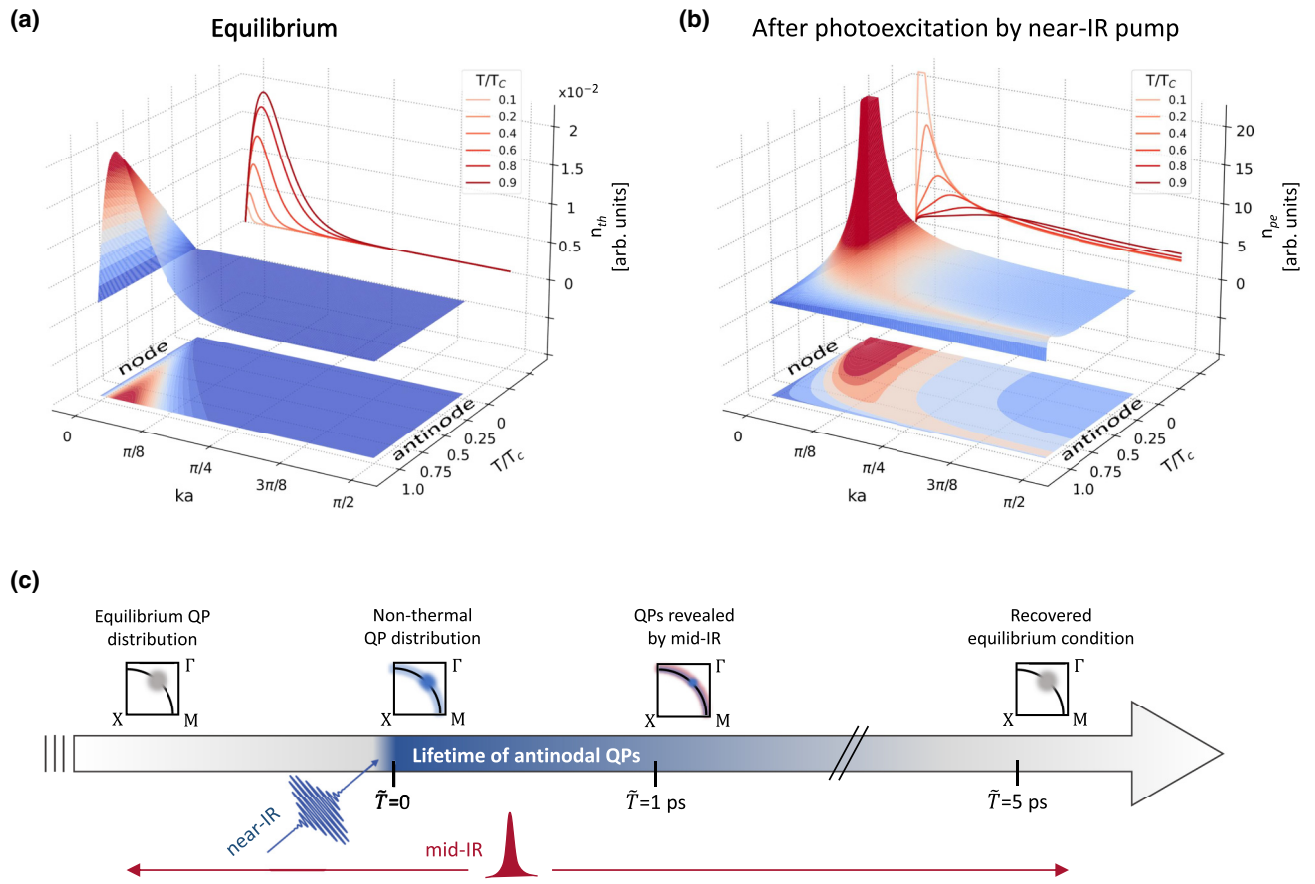

FIG. 7. Simulated momentum- and temperature-resolved quasiparticle distributions. (a) Equilibrium quasiparticle density (n_{th}) obtained by multiplying the QP density of states of a d-wave superconductor [80] by the quasiparticle Fermi-Dirac distribution. The red curves are cuts as a function of momentum at different temperatures listed in the legend. (b) Photoexcited quasiparticle density (n_{pe}) according to Eq. (4) for a temperature- and momentum-dependent gap $\Delta(k, T)$. For visual needs, the distribution has been cut at $n_{pe} = 20$. As showed in the red cuts, an amount of antinodal quasiparticles is photoexcited at all temperatures. (c) Sketch of the lifetime of the photoexcited antinodal QPs revealed by the mid-IR three-pulse spectroscopy.

1, thermal QPs are located only at low energies, namely at the nodes where $ka \sim 0$. As soon as the temperature increases and approaches T_C, thermal QPs populate states at higher energies and move away from the node. However, even at T_C, thermal excitations are not sufficient to populate the antinodal states. In the simulations we have considered $\Delta_{SC} = 75$ meV and $T_C = 90$ K.

In the three-pulse experiment, however, the mid-IR pump impinging on the sample does not interact with an equilibrium QP distribution, but instead with a nonthermal QP population previously injected by the near-IR pump according to Eq. (4). In order to introduce the momentum dependence of the gap amplitude, we rescaled the temperature-dependent gap in Eq. (4) as a function of k, so that $\Delta(k, T) = \Delta_{SC} \sin(ka) \tanh(1.75 \times \sqrt{\frac{T_C}{T} - 1})$. We highlight that this procedure, even though it neglects the k-dependent phonon distribution, is in general reliable since in the scattering events between QPs and impurities momentum is conserved. The resulting photoexcited QP density n_{pe} is plotted in Fig. 7(b) as a function of temperature and momentum. The simulation shows that photoinjected QPs populate states at all momenta, in agreement with previous ARPES findings [26,28].

The comparison between the equilibrium [Fig. 7(a)] and the nonthermal QP distribution [Fig. 7(b)] reveals that antinodal states can be populated only upon photoexcitation by an above-gap pump. Furthermore, as displayed in the temperature cuts in Fig. 7(b), the creation of antinodal QPs is expected at all temperature below T_C.

The two distinct scenarios in Figs. 7(a) and 7(b) can be singled out in the three-pulse experiment, where the order of arrival of the pumps discriminates two cases.

(1) If the mid-IR pump impinges before the near-IR one [Fig. 6(c)], the first pulse accelerates the condensate according to Eq. (5) and creates few low-energy ($\epsilon \ll \Delta_{SC}$) excitations. Since the sample is at nonzero temperature, the response is governed by absorption, i.e., by thermally-excited QPs [Fig. 7(a)]. When the second near-IR pulse arrives 1 ps later, additional QPs are created at higher energy and momentum [Fig. 7(b)]. The total response will therefore be that of the second pump only and can be described by Eq. (4), in which the photoexcitation intensity $\mathcal{E}_I$ is that of the near-IR pump alone, I_{NIR}. This is summarized in the sketches in the bottom of Fig. 6(c).

(2) When the order of arrival is swapped [Fig. 6(d)], however, there is a substantial amount of antinodal QPs

photoexcited by the first impinging near-IR pump, as shown in Fig. 7(b). This nonequilibrium QP distribution can absorb energy from the mid-IR pump, that − when impinging on the sample 1 ps later − can now couple to the previously excited nonthermal QPs. Again, the photoresponse is determined by Eq. (4), where $\mathcal{E}_I$ is now the sum of the absorbed energies from the first and the second pump, $I_{\mathrm{NIR}} + I_{\mathrm{MIR}}$. The dynamics measured is thus qualitatively similar to the one initiated by the photoexcitation with high photon energy alone, as observed in the extrapolated *SW* dynamics.

The fact that the differential response vanishes above the critical temperature [Figs. 6(e) and 6(f)] is a further confirmation that the difference found between high- and low-photon energy excitations is closely related to the presence of the SC gap. The closure of the gap at T_C suppresses the d-wave anisotropy and, in turn, the difference in the k-dependent QP distribution excited by the two pumps.

To conclude, in the three-pulse experiment the interaction with the mid-IR pump represents a means to probe the presence of antinodal QPs. Indeed, the response to subgap pulses is different whether or not the antinodal regions have been populated with QPs by the previous interaction with a high-energy pump, thus leading to a nonzero differential signal in the SC phase [Fig. 6(f)].

The mid-IR pump can then be used to probe the lifetime of the antinodal QP population. By tuning the delay $\tilde{T}$ between the two pumps, it is possible to track the recombination dynamics of previously excited QPs, that is pictorially illustrated in Fig. 7(c). At $\tilde{T} < 0$, mid-IR pulses interact with a thermal population of QPs located at the nodal region of the first Brillouin zone [leftmost sketch in Fig. 7(c)]. When the photoexcitation by the near-IR pump suddenly injects antinodal QPs, a non-null differential response emerges at $\tilde{T} > 0$. Importantly, by quantifying the differential response as a function of $\tilde{T}$, the lifetime of antinodal QPs can be extrapolated. In Fig. S12 in Ref. [52], we plot the integrated differential response below T_C, showing that it displays an exponentially decaying dynamics and vanishes at $\tilde{T} \sim 5$ ps. By fitting the data, we estimate a decay time of ~ 1.2 ps. Interestingly, this observation matches well the reported dynamics of the photoinduced gap filling in Bi2212 that has been related to the ultrafast melting of the condensate driven by phase fluctuations [63], hinting at a connection between the recombination rate of QPs and the recovery dynamics of phase coherence that calls for future experimental and theoretical investigations.

IV. CONCLUSIONS

We have presented a systematic study of the optical response of optimally doped $Bi_2Sr_2Ca_{0.92}Y_{0.08}Cu_2O_{8+\delta}$ to photoexcitation both above and below the antinodal gap. We have showed that the transient optical response in the visible range is different for the two pumps only below T_C, confirming that the amplitude of the superconducting gap provides a natural threshold energy for the formation of photoexcited quasiparticles.

By modeling the broadband transient reflectivity with a time-dependent Drude-Lorentz dielectric function, we found that the out-of-equilibrium response is ruled by the transient modification of an oscillator at 2 eV, whose dynamics qualitatively depends on the pump photon energy. Based on previous reports, this oscillator could involve both in-plane Cu-O charge-transfer excitations [2,46] and dd orbital transitions [47,50]. Our measurements do not clarify the nature of this transition, but we would rather focus on studying its transient response subsequently to photoexcitations with different photon energies.

The three-pulse scheme allowed us to further investigate the optical response of the sample due to the simultaneous photoexcitation by near-IR and mid-IR pumps and demonstrate that the overall response strongly depends on the sequence of the two perturbations in time only in the superconducting phase. We resorted to simulations based on the kinetic theory for superconductors [38] to show that the quasiparticle dynamics triggered by above- and below-gap photoexcitations are different below T_C, as a result of the anisotropy of the gap. In the presence of a d-wave gap, while near-IR pulses deliver sufficient energy to target the entire Fermi surface and accumulate nonthermal quasiparticles in the antinodal states that are inaccessible in equilibrium, mid-IR pulses mainly affect the nodal regions and only accelerate the condensate. Above the critical temperature, this dichotomy vanishes, and the momentum selectivity of the mid-IR excitation is suppressed. The mid-IR based three-pulse technique allowed us to capture the recombination dynamics of photoinjected quasiparticles, which was found compatible with previous time-resolved ARPES studies. Our findings highlight that excitation by pulses with suitable photon energy may provide a means to understand and control the nonequilibrium distribution of quasiparticles in momentum space.

ACKNOWLEDGMENTS

The authors acknowledge fruitful discussions with S. Dal Conte and J. Davis. This work was supported by the European Commission through the projects INCEPT (ERC-2015-STG, Grant No. 677488) and COBRAS (ERC-2019-PoC, Grant No. 860365). D.F. acknowledges funding from the MIUR through the PRIN Program No. 2017BZPKSZ and from the Gordon and Betty Moore Foundation through the grant CENTQC. The work at the University of Minnesota was funded by the U.S. Department of Energy through the University of Minnesota Center for Quantum Materials, under Grant No. DE-SC0016371. C.G. acknowledges financial support from MIUR through the PRIN 2020 (Prot. 2020JLZ52N 003) program and from the European Union - Next Generation EU through the MUR- PRIN2022 (Prot. 20228YCYY7) program. H.E. acknowledges support from the JSPS KAKENHI (No. JP19H05823). This research was undertaken thanks in part to funding from the Max Planck-UBC-UTokyo Centre for Quantum Material and the Canada First Research Excellence Fund, Quantum Material and Future Technologies Program. This project is also funded by the Natural Sciences and Engineering Research Council of Canada (NSERC); the Alexander von Humboldt Fellowship (A.D.); the Canada Research Chairs Program (A.D.); and the CIFAR Quantum Materials Program.

[1] M. J. Holcomb, J. P. Collman, and W. A. Little, Optical evidence of an electronic contribution to the pairing interaction in superconducting $Tl_2Ba_2Ca_2Cu_3O_{10}$, Phys. Rev. Lett. **73**, 2360 (1994).

[2] M. J. Holcomb, C. L. Perry, J. P. Collman, and W. A. Little, Thermal-difference reflectance spectroscopy of the high-temperature cuprate superconductors, Phys. Rev. B **53**, 6734 (1996).

[3] H. J. A. Molegraaf, C. Presura, D. van der Marel, P. H. Kes, and M. Li, Superconductivity-induced transfer of in-plane spectral weight in $Bi_2Sr_2CaCu_2O_{8+\delta}$, Science **295**, 2239 (2002).

[4] M. R. Norman and C. Pépin, The electronic nature of high temperature cuprate superconductors, Rep. Prog. Phys. **66**, 1547 (2003).

[5] A. V. Boris, N. N. Kovaleva, O. V. Dolgov, T. Holden, C. T. Lin, B. Keimer, and C. Bernhard, In-plane spectral weight shift of charge carriers in $YBa_2Cu_3O_{6.9}$, Science **304**, 708 (2004).

[6] D. N. Basov and T. Timusk, Electrodynamics of high-T_C superconductors, Rev. Mod. Phys. **77**, 721 (2005).

[7] W. N. Hardy, D. A. Bonn, D. C. Morgan, R. Liang, and K. Zhang, Precision measurements of the temperature dependence of λ in $YBa_2Cu_3O_{6.95}$: Strong evidence for nodes in the gap function, Phys. Rev. Lett. **70**, 3999 (1993).

[8] Z.-X. Shen, D. S. Dessau, B. O. Wells, D. M. King, W. E. Spicer, A. J. Arko, D. Marshall, L. W. Lombardo, A. Kapitulnik, P. Dickinson, S. Doniach, J. DiCarlo, A. G. Loeser, and C. H. Park, Anomalously large gap anisotropy in the a-b plane of $Bi_2Sr_2CaCu_2O_{8+\delta}$, Phys. Rev. Lett. **70**, 1553 (1993).

[9] J. R. Kirtley, C. C. Tsuei, J. Z. Sun, C. C. Chi, L. S. Yu-Jahnes, A. Gupta, M. Rupp, and M. B. Ketchen, Symmetry of the order parameter in the high-T_C superconductor $YBa_2Cu_3O_{7-\delta}$, Nature (London) **373**, 225 (1995).

[10] D. J. Van Harlingen, Phase-sensitive tests of the symmetry of the pairing state in the high-temperature superconductors—Evidence for d_{x2-y2} symmetry, Rev. Mod. Phys. **67**, 515 (1995).

[11] D. J. Scalapino, The case for d_{x2-y2} pairing in the cuprate superconductors, Phys. Rep. **250**, 329 (1995).

[12] C. M. Varma, Theory of the pseudogap state of the cuprates, Phys. Rev. B **73**, 155113 (2006).

[13] D. M. Newns and C. C. Tsuei, Fluctuating Cu–O–Cu bond model of high-temperature superconductivity, Nat. Phys. **3**, 184 (2007).

[14] T. P. Devereaux and R. Hackl, Inelastic light scattering from correlated electrons, Rev. Mod. Phys. **79**, 175 (2007).

[15] A. Damascelli, Z. Hussain, and Z.-X. Shen, Angle-resolved photoemission studies of the cuprate superconductors, Rev. Mod. Phys. **75**, 473 (2003).

[16] M. Zonno, F. Boschini, and A. Damascelli, Time-resolved ARPES on cuprates: Tracking the low-energy electrodynamics in the time domain, J. Electron Spectrosc. Relat. Phenom. **251**, 147091 (2021).

[17] L. Perfetti, P. A. Loukakos, M. Lisowski, U. Bovensiepen, H. Eisaki, and M. Wolf, Ultrafast electron relaxation in superconducting $Bi_2Sr_2CaCu_2O_{8+\delta}$ by time-resolved photoelectron spectroscopy, Phys. Rev. Lett. **99**, 197001 (2007).

[18] Y. H. Liu, Y. Toda, K. Shimatake, N. Momono, M. Oda, and M. Ido, Direct observation of the coexistence of the pseudogap and superconducting quasiparticles in $Bi_2Sr_2CaCu_2O_{8+y}$ by time-resolved optical spectroscopy, Phys. Rev. Lett. **101**, 137003 (2008).

[19] C. Giannetti, G. Coslovich, F. Cilento, G. Ferrini, H. Eisaki, N. Kaneko, M. Greven, and F. Parmigiani, Discontinuity of the ultrafast electronic response of underdoped superconducting $Bi_2Sr_2CaCu_2O_{8+\delta}$ strongly excited by ultrashort light pulses, Phys. Rev. B **79**, 224502 (2009).

[20] J. Graf, C. Jozwiak, C. L. Smallwood, H. Eisaki, R. A. Kaindl, D-H. Lee, and A. Lanzara, Nodal quasiparticle meltdown in ultrahigh-resolution pump-probe angle-resolved photoemission, Nat. Phys. **7**, 805 (2011).

[21] R. Cortés, L. Rettig, Y. Yoshida, H. Eisaki, M. Wolf, and U. Bovensiepen, Momentum-resolved ultrafast electron dynamics in superconducting $Bi_2Sr_2CaCu_2O_{8+\delta}$, Phys. Rev. Lett. **107**, 097002 (2011).

[22] C. L. Smallwood, J. P. Hinton, C. Jozwiak, W. Zhang, J. D. Koralek, H. Eisaki, D.-H. Lee, J. Orenstein, and A. Lanzara, Tracking cooper pairs in a cuprate superconductor by ultrafast angle-resolved photoemission, Science **336**, 1137 (2012).

[23] S. Dal Conte, C. Giannetti, G. Coslovich, F. Cilento, D. Bossini, T. Abebaw, F. Banfi, G. Ferrini, H. Eisaki, M. Greven, A. Damascelli, D. van der Marel, and F. Parmigiani, Disentangling the electronic and phononic glue in a high-T_C superconductor, Science **335**, 1600 (2012).

[24] G. Coslovich, C. Giannetti, F. Cilento, S. Dal Conte, T. Abebaw, D. Bossini, G. Ferrini, H. Eisaki, M. Greven, A. Damascelli, and F. Parmigiani, Competition between the pseudogap and superconducting states of $Bi_2Sr_2Ca_{0.92}Y_{0.08}Cu_2O_{8+\delta}$ single crystals revealed by ultrafast broadband optical reflectivity, Phys. Rev. Lett. **110**, 107003 (2013).

[25] F. Cilento, S. Dal Conte, G. Coslovich, S. Peli, N. Nembrini, S. Mor, F. Banfi, G. Ferrini, H. Eisaki, M. K. Chan, C. J. Dorow, M. J. Veit, M. Greven, D. van der Marel, R. Comin, A. Damascelli, L. Rettig, U. Bovensiepen, M. Capone, C. Giannetti, and F. Parmigiani, Photo-enhanced antinodal conductivity in the pseudogap state of high-T_C cuprates, Nat. Commun. **5**, 4353 (2014).

[26] C. L. Smallwood, W. Zhang, T. L. Miller, C. Jozwiak, H. Eisaki, D.-H. Lee, and A. Lanzara, Time-and momentum-resolved gap dynamics in $Bi_2Sr_2CaCu_2O_{8+\delta}$, Phys. Rev. B **89**, 115126 (2014).

[27] Y. Toda, S. Tsuchiya, M. Oda, T. Kurosawa, S. Katsumata, M. Naseska, T. Mertelj, and D. Mihailovic, Ultrafast transient reflectivity measurements of optimally doped $Bi_{2+x}Sr_{2-x}CaCu_2O_{8+\delta}$ with disorder, Phys. Rev. B **104**, 094507 (2021).

[28] F. Cilento, G. Manzoni, A. Sterzi, S. Peli, A. Ronchi, A. Crepaldi, F. Boschini, C. Cacho, R. Chapman, E. Springate, H. Eisaki, M. Greven, M. Berciu, A. F. Kemper, A. Damascelli, M. Capone, C. Giannetti, and F. Parmigiani, Dynamics of correlation-frozen antinodal quasiparticles in superconducting cuprates, Sci. Adv. **4**, 2 (2018).

[29] J. Demsar, Non-equilibrium phenomena in superconductors probed by femtosecond time-domain spectroscopy, J. Low Temp. Phys. **201**, 676 (2020).

[30] D. Fausti, R. I. Tobey, N. Dean, S. Kaiser, A. Dienst, M. C. Hoffmann, S. Pyon, T. Takayama, H. Takagi, and A. Cavalleri, Light-induced superconductivity in a stripe-ordered cuprate, Science **331**, 189 (2011).

[31] S. Kaiser, C. R. Hunt, D. Nicoletti, W. Hu, I. Gierz, H. Y. Liu, M. Le Tacon, T. Loew, D. Haug, B. Keimer, and A. Cavalleri,

Optically induced coherent transport far above T_C in underdoped $YBa_2Cu_3O_{6+\delta}$, Phys. Rev. B **89**, 184516 (2014).

[32] W. Hu, S. Kaiser, D. Nicoletti, C. R. Hunt, I. Gierz, M. C. Hoffmann, M. Le Tacon, T. Loew, B. Keimer, and A. Cavalleri, Optically enhanced coherent transport in $YBa_2Cu_3O_{6.5}$ by ultrafast redistribution of interlayer coupling, Nat. Mater. **13**, 705 (2014).

[33] E. Casandruc, D. Nicoletti, S. Rajasekaran, Y. Laplace, V. Khanna, G. D. Gu, J. P. Hill, and A. Cavalleri, Wavelength-dependent optical enhancement of superconducting interlayer coupling in $La_{1.885}Ba_{0.115}CuO_4$, Phys. Rev. B **91**, 174502 (2015).

[34] M. Mitrano, A. Cantaluppi, D. Nicoletti, S. Kaiser, A. Perucchi, S. Lupi, P. Di Pietro, D. Pontiroli, M. Riccò, S. R. Clark, D. Jaksch, and A. Cavalleri, Possible light-induced superconductivity in K_3C_{60} at high temperature, Nature (London) **530**, 461 (2016).

[35] F. Giusti, A. Marciniak, F. Randi, G. Sparapassi, F. Boschini, H. Eisaki, M. Greven, A. Damascelli, A. Avella, and D. Fausti, Signatures of enhanced superconducting phase coherence in optimally doped $Bi_2Sr_2Y_{0.08}Ca_{0.92}Cu_2O_{8+\delta}$ driven by midinfrared pulse excitations, Phys. Rev. Lett. **122**, 067002 (2019).

[36] G. M. Eliashberg, Inelastic electron collisions and nonequilibrium stationary states in superconductors, Sov. J. Exp. Theor. Phys. **34**, 668 (1972).

[37] A. I. Larkin and Y. U. N. Ovchinnikov, Nonlinear effects during vortex motion in superconductors, Sov. J. Exp. Theor. Phys. **73**, 299 (1977).

[38] V. V. Kabanov, J. Demsar, B. Podobnik, and D. Mihailovic, Quasiparticle relaxation dynamics in superconductors with different gap structures: Theory and experiments on $YBa_2Cu_3O_{7-\delta}$, Phys. Rev. B **59**, 1497 (1999).

[39] H. Eisaki, N. Kaneko, D. L. Feng, A. Damascelli, P. K. Mang, K. M. Shen, Z.-X. Shen, and M. Greven, Effect of chemical inhomogeneity in bismuth-based copper oxide superconductors, Phys. Rev. B **69**, 064512 (2004).

[40] G. Yu, Y. Li, E. M. Motoyama, and M. Greven, A universal relationship between magnetic resonance and superconducting gap in unconventional superconductors, Nat. Phys. **5**, 873 (2009).

[41] A. Montanaro, F. Giusti, M. Colja, G. Brajnik, A. M. A. Marciniak, R. Sergo, D. De Angelis, F. Glerean, G. Sparapassi, G. Jarc, S. Carrato, G. Cautero, and D. Fausti, Visible pump–midinfrared pump–broadband probe: Development and characterization of a three-pulse setup for single-shot ultrafast spectroscopy at 50 kHz, Rev. Sci. Instrum. **91**, 073106 (2020).

[42] S. Uchida *et al.*, Optical spectra of $La_{2-x}Sr_xCuO_4$: Effect of carrier doping on the electronic structure of the CuO_2 plane, Phys. Rev. B **43**, 7942 (1991).

[43] A. Comanac *et al.*, Optical conductivity and the correlation strength of high-temperature copper-oxide superconductors, Nat. Phys. **4**, 287 (2008).

[44] H. Eskes, M. B. J. Meinders, and G. A. Sawatzky, Anomalous transfer of spectral weight in doped strongly correlated systems, Phys. Rev. Lett. **67**, 1035 (1991).

[45] L. de' Medici, X. Wang, M. Capone, and A. J. Millis, Correlation strength, gaps, and particle-hole asymmetry in high-T_C cuprates: A dynamical mean-field study of the three-band copper-oxide model, Phys. Rev. B **80**, 054501 (2009).

[46] C. Giannetti, F. Cilento, S. Dal Conte, G. Coslovich, G. Ferrini, H. Molegraaf, M. Raichle, R. Liang, H. Eisaki, M. Greven, A. Damascelli, D. van der Marel, and F. Parmigiani, Revealing the high-energy electronic excitations underlying the onset of high-temperature superconductivity in cuprates, Nat. Commun. **2**, 353 (2011).

[47] D. Salamon, R. Liu, M. V. Klein, M. A. Karlow, S. L. Cooper, S-W. Cheong, W. C. Lee, and D. M. Ginsberg, Large-shift raman scattering in insulating parent compounds of cuprate superconductors, Phys. Rev. B **51**, 6617 (1995).

[48] G. Ghiringhelli, N. B. Brookes, E. Annese, H. Berger, C. Dallera, M. Grioni, L. Perfetti, A. Tagliaferri, and L. Braicovich, Low energy electronic excitations in the layered cuprates studied by copper L_3 resonant inelastic x-ray scattering, Phys. Rev. Lett. **92**, 117406 (2004).

[49] M. Moretti Sala, V. Bisogni, C. Aruta, G. Balestrino, H. Berger, N. B. Brookes, G. M. de Luca, D. Di Castro, M. Grioni, M. Guarise, P. G. Medaglia, F. Miletto Granozio, M. Minola, P. Perna, M. Radovic, M. Salluzzo, T. Schmitt, K. J. Zhou, L. Braicovich, and G. Ghiringhelli, Energy and symmetry of dd excitations in undoped layered cuprates measured by Cu L_3 resonant inelastic x-ray scattering, New J. Phys. **13**, 043026 (2011).

[50] F. Barantani, M. K. Tran, I. Madan, I. Kapon, N. Bachar, T. C. Asmara, E. Paris, Y. Tseng, W. Zhang, Y. Hu, E. Giannini, G. Gu, T. P. Devereaux, C. Berthod, F. Carbone, T. Schmitt, and D. van der Marel, Resonant inelastic x-ray scattering study of electron-exciton coupling in high-T_C cuprates, Phys. Rev. X **12**, 021068 (2022).

[51] F. Barantani, C. Berthod, and D. van der Marel, Can dd excitations mediate pairing? Physica C (Amsterdam, Neth.) **613**, 1354321 (2023).

[52] See Supplemental Material at http://link.aps.org/supplemental/10.1103/PhysRevB.110.125102 for details on the equilibrium fit of the reflectivity; differential fits of the out-of-equilibrium reflectivity in the superconducting, pseudogap and normal phases; fluence-dependent studies and differential fits for the mid-IR pump, near-IR pump and the probe; temperature-dependent reflectivity maps and differential fits; temperature-dependent dynamics of the spectral weight; details on the double-pump measurement in the superconducting phase and extrapolated dynamics of the spectral weight and central frequency of the 2 eV oscillator. It also contains Refs. [53–57].

[53] F. Cilento, Non-equilibrium phase diagram of $Bi_2Sr_2Y_{0.08}Ca_{0.92}Cu_2O_{8+\delta}$ cuprate superconductors revealed by ultrafast optical spectroscopy, Ph.D. Thesis, University of Trieste, 2011.

[54] E. van Heumen, E. Muhlethaler, A. B. Kuzmenko, H. Eisaki, W. Meevasana, M. Greven, and D. van der Marel, Optical determination of the relation between the electron-Boson coupling function and the critical temperature in high-T_C cuprates, Phys. Rev. B **79**, 184512 (2009).

[55] A. S. Mishchenko, N. Nagaosa, Z.-X. Shen, G. De Filippis, V. Cataudella, T. P. Devereaux, C. Bernhard, K. W. Kim, and J. Zaanen, Charge dynamics of doped holes in high-T_C cuprate superconductors: A clue from optical conductivity, Phys. Rev. Lett. **100**, 166401 (2008).

[56] G. De Filippis, V. Cataudella, A. S. Mishchenko, C. A. Perroni, and N. Nagaosa, Optical conductivity of a doped Mott insulator: The interplay between correlation and electron-phonon interaction, Phys. Rev. B **80**, 195104 (2009).

[57] Y. Li, M. Le Tacon, Y. Matiks, A. V. Boris, T. Loew, C. T. Lin, Lu Chen, M. K. Chan, C. Dorow, L. Ji, N. Barišić, X. Zhao, M. Greven, and B. Keimer, Doping-dependent photon scattering resonance in the model high-temperature superconductor $HgBa_2CuO_{4+\delta}$ revealed by raman scattering and optical ellipsometry, Phys. Rev. Lett. **111**, 187001 (2013).

[58] A. B. Kuzmenko, Kramers–Kronig constrained variational analysis of optical spectra, Rev. Sci. Instrum. **76**, 083108 (2005).

[59] S. I. Mirzaei, D. Stricker, J. N. Hancock, C. Berthod, A. Georgesa, E. van Heumena, M. K. Chan, X. Zhao, Y. Li, M. Greven, N. Barišić, and D. van der Marel, Spectroscopic evidence for Fermi liquid-like energy and temperature dependence of the relaxation rate in the pseudogap phase of the cuprates, Proc. Nat. Acad. Sci. USA **110**, 5774 (2013).

[60] F. Giusti, A. Montanaro, A. Marciniak, F. Randi, F. Boschini, F. Glerean, G. Jarc, H. Eisaki, M. Greven, A. Damascelli, A. Avella, and D. Fausti, Anisotropic time-domain electronic response in cuprates driven by midinfrared pulses, Phys. Rev. B **104**, 125121 (2021).

[61] Y. Toda, T. Mertelj, P. Kusar, T. Kurosawa, M. Oda, M. Ido, and D. Mihailovic, Quasiparticle relaxation dynamics in underdoped $Bi_2Sr_2CaCu_2O_{8+\delta}$ by two-color pump-probe spectroscopy, Phys. Rev. B **84**, 174516 (2011).

[62] S. Parham, H. Li, T. J. Nummy, J. A. Waugh, X. Q. Zhou, J. Griffith, J. Schneeloch, R. D. Zhong, G. D. Gu, and D. S. Dessau, Ultrafast gap dynamics and electronic interactions in a photoexcited cuprate superconductor, Phys. Rev. X **7**, 041013 (2017).

[63] F. Boschini, E. H. da Silva Neto, E. Razzoli, M. Zonno, S. Peli, R. P. Day, M. Michiardi, M. Schneider, B. Zwartsenberg, P. Nigge, R. D. Zhong, J. Schneeloch, G. D. Gu, S. Zhdanovich, A. K. Mills, G. Levy, D. J. Jones, C. Giannetti, and A. Damascelli, Collapse of superconductivity in cuprates via ultrafast quenching of phase coherence, Nat. Mater. **17**, 416 (2018).

[64] T. Kurosawa Madan, Y. Toda, M. Oda, T. Mertelj, P. Kusar, and D. Mihailovic, Separating pairing from quantum phase coherence dynamics above the superconducting transition by femtosecond spectroscopy, Sci. Rep. **4**, 5656 (2014).

[65] F. Giusti, Intensity and Fluctuation Dynamics in Pump-Probe Experiments in Complex Material, Ph.D. Thesis, University of Trieste, 2019.

[66] C. Giannetti, M. Capone, D. Fausti, M. Fabrizio, F. Parmigiani, and D. Mihailovic, Ultrafast optical spectroscopy of strongly correlated materials and high-temperature superconductors: A nonequilibrium approach, Adv. Phys. **65**, 58 (2016).

[67] S. Peli, S. Dal Conte, R. Comin, N. Nembrini, A. Ronchi, P. Abrami, F. Banfi, G. Ferrini, D. Brida, S. Lupi, M. Fabrizio, A. Damascelli, M. Capone, G. Cerullo, and C. Giannetti, Mottness at finite doping and charge instabilities in cuprates, Nat. Phys. **13**, 806 (2017).

[68] D. Pelc, P. Popčević, M. Požek, M. Greven, and N. Barišić, Unusual behavior of cuprates explained by heterogeneous charge localization, Sci. Adv. **5**, eaau4538 (2019).

[69] D. Pelc, M. J. Veit, C. J. Dorow, Y. Ge, N. Barišić, and M. Greven, Resistivity phase diagram of cuprates revisited, Phys. Rev. B **102**, 075114 (2020).

[70] M. Tinkham, *Introduction to superconductivity* (Courier Corporation, North Chelmsford, MA, 2004).

[71] M. P. Kemoklidze and L. P. Pitaevskii, Dynamics of a superfluid fermi gas at finite temperatures, Sov. J. Exp. Theor. Phys. **52**, 1556 (1967).

[72] V. F. Elesin and Y. V. Kopaev, Superconductors with excess quasiparticles, Sov. Phys. Usp. **24**, 116 (1981).

[73] V. V. Kabanov, J. Demsar, and D. Mihailovic, Kinetics of a superconductor excited with a femtosecond optical pulse, Phys. Rev. Lett. **95**, 147002 (2005).

[74] A. G. Aronov, M. A. Zelikman, and B. Z. Spivak, Nonequilibrium excitations in superconductors and phonon fluorescence, Sov. Phys. Solid State **18**, 1286 (1976).

[75] W. H. Parker, Modified heating theory of nonequilibrium superconductors, Phys. Rev. B **12**, 3667 (1975).

[76] A. Rothwarf and B. N. Taylor, Measurement of recombination lifetimes in superconductors, Phys. Rev. Lett. **19**, 27 (1967).

[77] O. Betbeder-Matibet and P. Nozieres, Transport equations in clean superconductors, Ann. Phys. **51**, 392 (1969).

[78] G. M. Eliashberg, Film superconductivity stimulated by a high-frequency field, Sov. J. Exp. Theor. Phys. Lett. **11**, 186 (1970).

[79] M. Beck, I. Rousseau, M. Klammer, P. Leiderer, M. Mittendorff, S. Winnerl, M. Helm, G. N. Gol'tsman, and J. Demsar, Transient increase of the energy gap of superconducting nbn thin films excited by resonant narrow-band Terahertz Pulses, Phys. Rev. Lett. **110**, 267003 (2013).

[80] H. Won and K. Maki, *d*-wave superconductor as a model of high-T_c superconductors, Phys. Rev. B **49**, 1397 (1994).